ORIGINAL PAPER

Cavitation Bubble Measurement in Tribological Contacts Using Digital Holographic Microscopy

Tian Tang · Nick Morris · Jeremy Coupland · Laura Arevalo

Abstract The use of advanced measurement techniques such as the digital holography method described in this paper improves the understanding of the cavitation phenomenon in tribological contacts such as the sliding contact of the piston ring–cylinder liner conjunction. The paper describes the use of digital holography measurement technique to measure cavitation bubble formation and thickness. The position of observed lubricant film rupture preceding the cavitation region is compared with some commonly predicted boundary often used with Reynolds equation. The experimental results indicate that the Reynolds and Elrod boundary conditions are the most suitable for the investigated sliding contact conditions.

List of symbols

a	Amplitude distribution
A	Bearings contact areas
D	Width of the cylindrical lens
F	Hydrodynamic lift force
h	Film thickness
h_m	Minimum film thickness
h_∞	Asymptotic film height far down stream of the separation point
I	Intensity of the hologram
k	Cavitation model switching parameter
L	Length of the cylindrical lens
n_0	Refractive index of oil
N	Capillary number
NA	Numerical aperture of the microscope
$\mathbf{o}$	Complex object field
p	Hydrodynamic pressure
P_{cav}	Cavitation pressure
P_{in}	Inlet pressure
U	Bearing sliding velocity
$\mathbf{r}$	Complex reference field
R	Radius of the cylindrical lens
R_1	Maximum radius of curvature of the bubble
R_2	Minimum radius of curvature of the bubble
R_a	Surface roughness
T	Bubble thickness
W	Constant load on the cylindrical lens
x_{cav}	Film rupture position
x_{in}	Inlet position

Greek symbols

γ	Surface tension
ε	Load convergence criteria
η	Lubricant viscosity
λ	Laser wavelength
ξ	Damping coefficient
φ	Phase
χ	Load balance parameter

T. Tang (✉) · N. Morris · J. Coupland
Department of Mechanical and Manufacturing Engineering,
Loughborough University, Loughborough, UK
e-mail: T.Tang2@lboro.ac.uk

N. Morris
e-mail: N.J.Morris@lboro.ac.uk

J. Coupland
e-mail: J.M.Coupland@lboro.ac.uk

L. Arevalo
Aragón Institute of Engineering Research, University
of Zaragoza, Saragossa, Spain
e-mail: Larevalo@unizar.es

1 Introduction

Driven by the need for bearings with increased load capacity and reduced frictional losses and wear, lubricating flow has been the subject of extensive studies for well over a century [1]. Of particular current interest is the role that cavitation plays in the performance of piston rings, journal and sliding bearings [2]. Cavities are formed when the gas pressure drops below either the lubricant vaporisation pressure (vaporous cavitation) or the saturation pressure of dissolved air (gaseous cavitation). It is well known that cavitation can negate sub-cavity pressures in divergent contact regions. However, its detrimental effect on the wear of bearing surfaces through the process of erosion remains a topic of debate [3].

In this paper, the measurement of cavitation generated by a plane surface sliding over a cylindrical component is considered as shown in Fig. 1. This geometry has been well defined in both experimental and analytical studies as it is analogous to the geometry of a piston ring–cylinder liner conjunction [4]. The configuration was chosen for this work because it is easily fabricated out of precise yet inexpensive optical components facilitating the measurement of cavitation using interferometric methods.

Following the pioneering work of Reynolds in [5], there has been significant effort to produce suitable outlet boundary conditions for Reynolds-based lubrication models. Review papers by Dowson and Taylor [6] and Majumdar [7] and Braun [2] provide an excellent summary of the intervening investigations into cavitation in bearings.

If the inlet and outlet pressures at the edges of the bearing are assumed to be atmospheric (the full-Sommerfeld boundary condition), then the direct solution of Reynolds equation reveals that the fluid must support sub-ambient pressures and the bearing cannot support a load without cavitation. Gümbel [8] was the first to account for film rupture by considering the full film region to terminate at the minimum clearance, negating any sub-cavity pressures (half-Sommerfeld condition). Although mathematically straightforward, this assumption is not physical and does not account for flow continuity.

In order to satisfy flow continuity, there are essentially two possibilities: either the flow must pass around multiple cavities (in "streamers") or it must flow over or under a single cavity within the diverging section of the contact. Both of these theories have been studied extensively. Multiple cavities between the bearing surfaces were proposed independently by Swift [9] and Stieber [10] who suggested that, for cavities that extend into the ambient region (i.e. open cavities), Reynolds equation could be used to describe the pressure with the additional boundary condition that both the pressure is equal to the outlet pressure and its gradient diminishes. The assumption of multiple cavities between the bearing surfaces was also progressed in a series of papers by Floberg [11], Jacobson and Floberg [12], Olsson [13] and Floberg [14] and together this work is collectively referred to as the JFO theory boundary conditions. For the first time, JFO theory presented the reformation boundary conditions necessary to describe closed cavities and a corresponding change in the predicted load-carrying capacity. Efficient algorithms to calculate the bearing characteristics iteratively were later proposed by Elrod [15, 16] and later by Vijayaraghavan and Keith [17].

The alternative notion, that the lubricant flows over or under a single cavity, has also been discussed and revisited several times. Birkhoff and Hays [18] recognised that according to the pressure distribution predicted by Reynolds equation, a flow reversal is predicted at a point in the diverging region. At this point, they propose that the flow separates to form a single cavity. This concept was extended considerably by Coyne and Elrod [19, 20] who introduced the influence of surface tension, gravity and inertia. Although the gravity and inertial effects are small, the surface tension causes a substantial pressure difference between the cavity and the surrounding fluid. This allows the cavity to "retreat" into the low-pressure region further from the point of minimum clearance and a corresponding decrease in load-carrying capability is predicted. A more recent analysis of gas cavity bubble shear and lubricant gas transfer conducted by Groper and Etsion [21] also used the single-cavity assumption.

Significant efforts have been made to experimentally investigate the nature of cavitation in bearings [22–26]. Pressure data are often measured experimentally to gain an understanding of the contact conditions. Dowson et al. [22] and Etsion and Ludwig [23] investigated the hydrodynamic film rupture in non-conformal contacts and pressure fluctuation in the region of cavitation in journal bearings, respectively. Both papers employed a combination of photography and pressure measurements techniques. Indeed, use of photography has been widely used to investigate cavitation bubbles in many bearings types. Dowson [24] observed cavitation bubbles in the lubricant between a fixed convex lens and a sliding steel plane surface. Braun and Hendricks [25] photographed cavitation bubbles in a
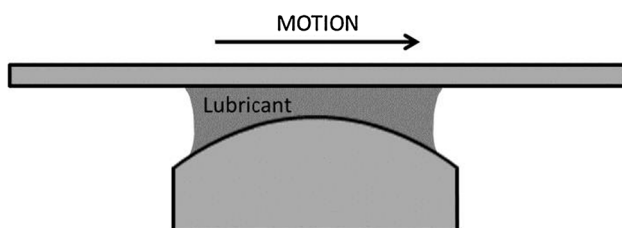

Fig. 1 Plano–cylindrical sliding bearing geometry

journal bearing. Both studies viewed the bearing from above showing that cavitation occurs in the divergent region, while the fluid flows out of the contact through lubricant streamers between the fingers like bubbles. Using photographs taken from different angles, Heshmat [26] observations suggest that a continuous sub-layer is present on the moving surface in the cavitation region. Dellis and Arcoumanis [27] have studied the different bubble shapes formed in the lubricant film of a piston ring assembly also using photographic methods. More recently, Vladescu et al. [28] have used a laser-induced fluorescence to qualitatively visualise cavitation phenomena in surface-textured sliding bearings.

In this paper, the use of digital holographic microscopy is to realise high-resolution measurements of cavities within sliding bearings for the first time. A precision slide capable of bidirectional motion is used to drive glass-bearing surfaces fabricated from precision grade optical components. It is shown how the holographic recordings can be analysed to extract the bubble thickness with a lateral resolution of a few microns and a thickness resolution of a few tens of nanometres. Results from a series of experiments are discussed with reference to the theoretical models of lubricating flows.

2 Experimental Configuration

In order to gain further understanding of the role of cavitation bubbles in lubricating flow, the cylinder–plane sliding contact configuration, shown in Fig. 2, was constructed from precision grade optical components with a prescribed surface form error (<50 nm) and surface roughness ($R_a < 1$ nm).

The plane glass component is driven by a motorised translation stage capable of bidirectional motion with controlled speed (0–2.3 mm/s) and acceleration (up to 1.5 mm/s^2). The cylindrical component (radius $R = 13.25$ mm, width $D = 12.5$ mm and length $L = 25$ mm) is fixed on a stationary metal surface. The lubricating oil used in this study is additive-free, high-viscosity classic green gear oil (SAE 140) with a viscosity $\eta = 1.508$ Pa s measured at room temperature (20 °C). The sliding plane glass is entirely supported by the hydrodynamic film entrained into the contact with the cylindrical lens, when a constant load of $W = 2.65$ N is applied to the cylindrical lens.

3 Digital Holographic Microscopy

The digital holographic microscope that was used for this study is shown in Fig. 3. The plane wave from a Q-swithched, diode-pumped, frequency-doubled Nd:YLF laser of wavelength $\lambda = 523$ nm is divided into reference and object beams using a 50:50 beam splitter. The bearing is illuminated by the plane wave that constitutes the object beam and its image magnified by 80× using a microscope objective with NA = 0.55. The image is mixed with a diverging reference wave from the same source such that a near-image-plane hologram is recorded on a CCD sensor with 4,008 × 2,672, 9.0 µm square pixels. The camera is capable of 5.22 frames per second, however, by using commercially available CCD sensors with higher frame rates; it would be possible to investigate the initiation of cavitation and also cavitation in transient contacts.
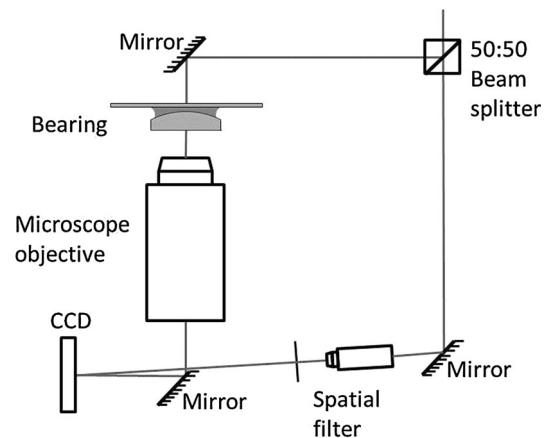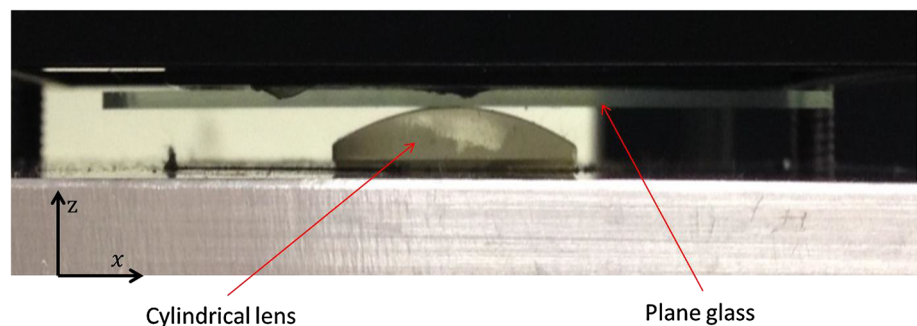
Fig. 3 Digital holographic microscope

Fig. 2 Experimental configuration

Details of this microscope and the reconstruction process can be found elsewhere [29, 30]. However, it is worth considering some of the fundamental attributes of a coherent imaging system before proceeding.

The fundamental difference between incoherent and coherent imaging is illustrated by Fig. 4 which shows the intensity pattern recorded by the CCD. An enlargement of the black square reveals the fringes caused by the interference of the object beam and the reference beam. It is the position and contrast of these fringes that contain the information that is related to the amplitude and the phase of the recorded wavefront.

In order to reconstruct the hologram, the following demodulation process is used. If the complex field due to the object beam through the glass bearing is $\mathbf{o}(x, y)$ and the complex field due to the reference beam is $\mathbf{r}(x, y)$, then the intensity of Fig. 4, $I(x, y)$, can be written as

$$
\begin{aligned}
I(x,y) &= |\mathbf{r}(x,y) + \mathbf{o}(x,y)|^2 \\
&= |\mathbf{r}(x,y)|^2 + |\mathbf{o}(x,y)|^2 + \mathbf{o}(x,y)^*\mathbf{r}(x,y) \\
&\quad + \mathbf{o}(x,y)\mathbf{r}(x,y)^*
\end{aligned} \tag{1}
$$

In an off-axis hologram such as this, each of the terms has a different spatial bandwidth which means that the terms in Eq. (1) can be separated in the frequency domain.

Figure 5 is the absolute value of the Fourier transform of Fig. 4 which illustrates the frequency bands corresponding to the different terms in Eq. (1). The centre circle represents the band of first two terms in Eq. (1), while the two bright regions in the corners of the spectrum represent the holographic image of the third and fourth terms, respectively. Holographic reconstruction can be achieved using the Fourier transform of either the third or fourth term.
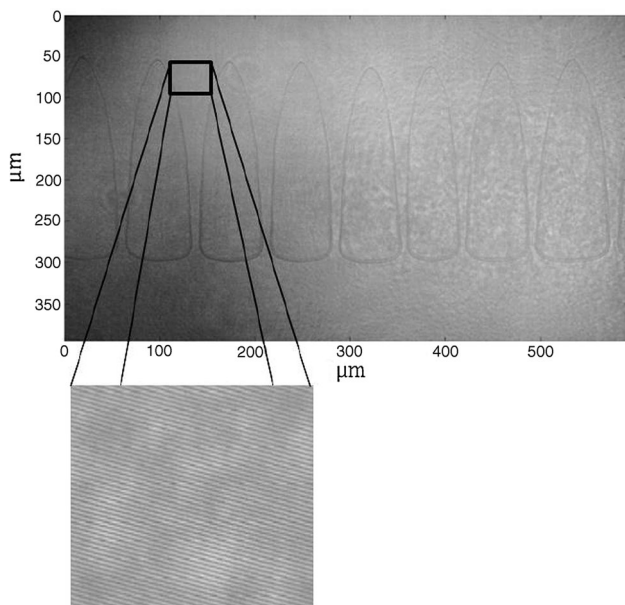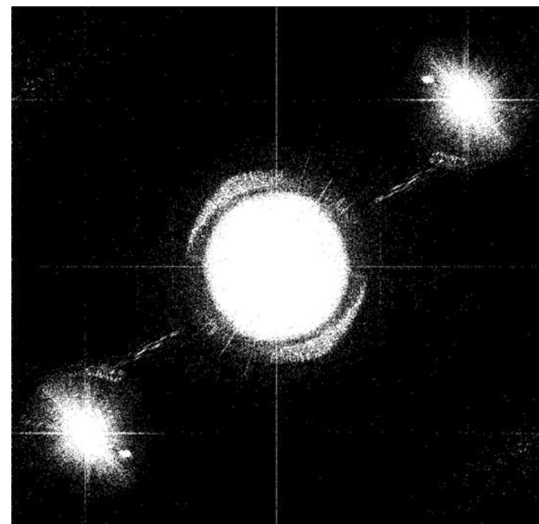

Fig. 5 Fourier spectrum of the hologram

Since the reference field is known, the phase and amplitude of object field can be calculated. Hence, the reconstruction is simply a filtered version of the recorded intensity pattern.

A major advantage of coherent imaging using digital holographic microscopy rather than its incoherent counterpart is that both the recorded fields are available for further analysis. That is, the recovered object field, $\mathbf{o}(x, y)$, can be written as,

$$
\mathbf{o}(x, y) = a(x, y) \exp(\mathbf{j}\phi(x, y)) \tag{2}
$$

where $\phi(x, y)$ is the phase and $a(x, y)$ the amplitude distribution. In this study, the phase is the most important parameter as illustrated in Fig. 6 which shows the phase of the demodulated hologram shown in Fig. 4. It can be seen that the cavitation bubbles are now revealed, but there are underlying fringes that are principally due to wavefront aberration in the illuminating beam. In order to remove this contribution, it is useful to subtract the phase distribution

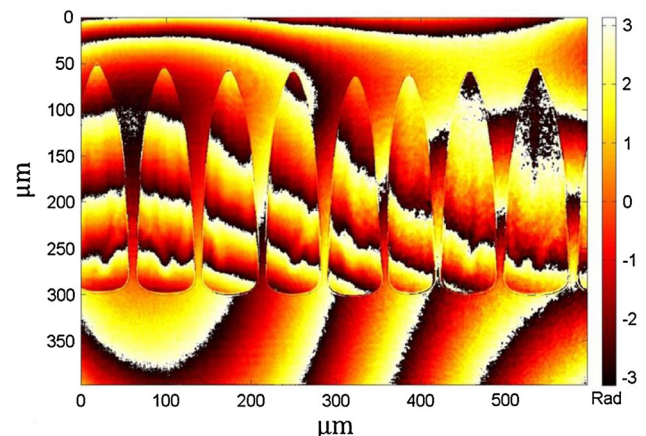Fig. 4 Holographic recording of cavitation

Fig. 6 Demodulated phase map

recovered from a holographic recording of the apparatus when there is no cavitation (i.e. when the slide is stationary).

An example of the subtracted phase is shown in Fig. 7. The information revealed in this and other similar images will now be discussed with reference to the theoretical models of lubricating flows.

4 Results and Analysis

In the experiment, regular shape bubbles such as those shown in Fig. 7 were observed after a short time after start-up when the slide is moving at constant velocity towards the top of its speed range, in this case after approximately 2 s when it is travelling at 2.3 mm/s. The multiple regularly spaced cavitation bubbles have closed cavities as suggested by the JFO theory. The bubbles shown in Fig. 7 are generated as result of the motorised translation stage moving from top to bottom of the image. The distances on the vertical axis are taken from the point of minimum clearance. Therefore in the region, where the bubbles are formed, there is an increasing clearance between the bearing surfaces. The gap between the bubbles (the streamer) becomes smaller as the distance from the centre increases. This is in accord with the continuity of mass flow. The bubble thickness measurements are now considered in detail.

4.1 Thickness Measurement

The fringes in Fig. 7 are due to the difference in refractive indices between the gas inside the bubbles and the surrounding lubricant. Using these fringes, a quantitative measurement of bubble thickness can be made. The fringes in the bubbles represent the change in phase $\Delta\varphi(x, y)$,
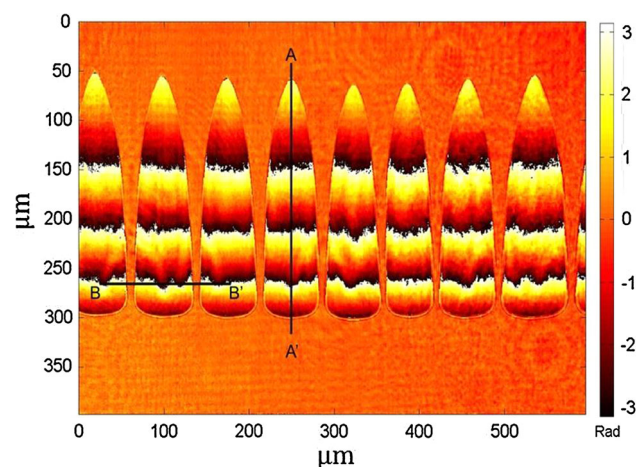
which are due to the propagation of the illuminating wave through a distance $T(x, y)$ in the cavitation bubble. The relationship between $\Delta\varphi(x, y)$ and $T(x, y)$ is given to a good approximation by:

$$\Delta\varphi(x,y) = \frac{2\pi}{\lambda}(n_0 - 1)T(x, y) \qquad (3)$$

where λ is the laser wave length, n_0 is the reflective index of the lubricant ($n_0 = 1.499$). Figure 8 shows the cavitation bubble thickness profile along the line A–A' as shown in Fig. 7.

Figure 8 shows that at the upstream end of the bubble, the thickness jumps to about 0.3 μm. Then the bubble thickness increases to around 4.5 μm and there is another step change in thickness. The significance of this measurement is discussed later. However, it is also noted that the phase of the cavitation bubble varies along the path B-B', and the corresponding thickness using Eq. (3) is shown in Fig. 9.

The variation of bubble thickness along the line B-B' is a strong evidence that the lubricant flows above or below the cavity. It is noted that this evidence supports the hypothesis of Coyne and Elrod, although there are clearly multiple cavities as proposed by the JFO model. It also noted that the possibility of fluid flowing on both the upper and lower sides of the cavity (i.e. a free bubble) can be excluded by an argument based on surface tension as follows.

Returning to the thickness variations along the line A-A', it is noted that the bubble thickness at its inception is approximately 0.3 μm. According to Laplace–Young [31] equation, the pressure drop, Δp, across the bubble interface is given by

$$\Delta p = \gamma\left(\frac{1}{R_1} + \frac{1}{R_2}\right) \qquad (4)$$

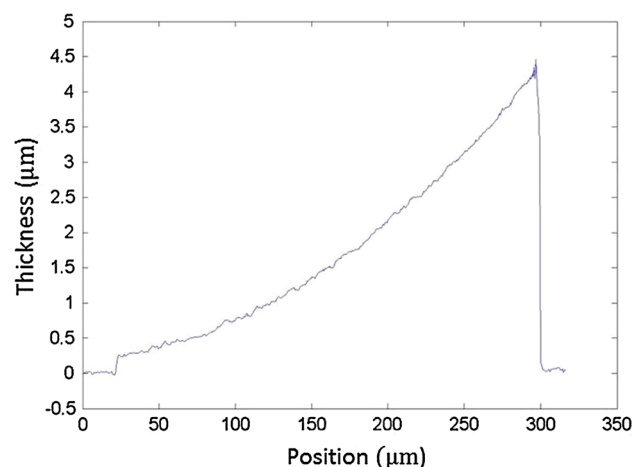
Fig. 7 Subtracted phase map

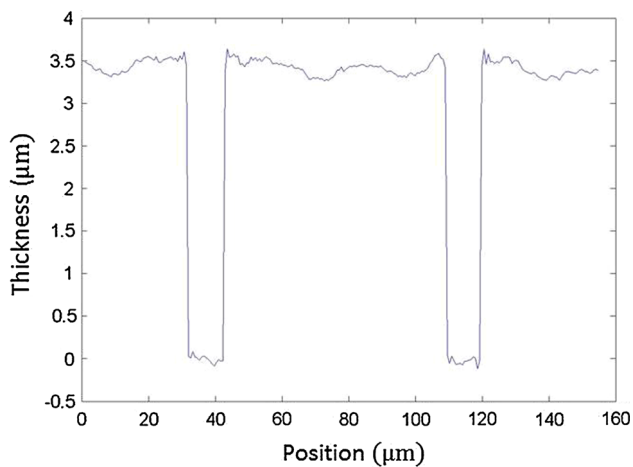**Fig. 8** Bubble thickness along line A–A' in Fig. 7

Fig. 9 Bubble thickness along line B–B′ in Fig. 7

where γ is the surface tension (in this case 0.03 N/m), and R_1, R_2 are the principal radii of curvature. It is straightforward to show that a free bubble of this thickness would have a Laplace pressure in excess of two atmospheres and would therefore dissolve into the lubricant. It can therefore be concluded that the bubble is in direct contact with one surface and it is reasonable to expect that to be the lower, cylindrical surface since the pressure distribution is stationary with respect to this boundary. The results provide a quantified measurement of the observations of Heshmet [26] and Estsion and Ludwig [23].

4.2 Position Measurements

The ability of system to reverse direction allows measurements of bubble position (or the lubricant rupture point) relative to the point of minimum clearance. In order to do this, two holograms, corresponding to forward and reverse motion at a given velocity, are added together.

Figure 10 shows the addition phase distribution of forward and reverse motion at a velocity of 1.5 mm/s. The corresponding bubble thickness on both sides can be measured along line C–C′ and is shown in Fig. 11. It is interesting to fit the geometry of cylindrical surface (radius = 13.25 mm) to the thickness measurement (the dotted curve on Fig. 11). It is clear that the bubble thickness curvature is almost identical to the curvature of the cylindrical surface. This evidence further supports the hypothesis that the bubble is in contact with the lower, cylindrical surface.

The symmetry of the added holograms allows for the estimation of the position of the line of minimum clearance and the onset of cavitation relative to this line. Figure 12a–d shows similar holograms for a range of different velocities. The position of minimum clearance (dotted line) and the onset of cavitation (solid lines) are illustrated for
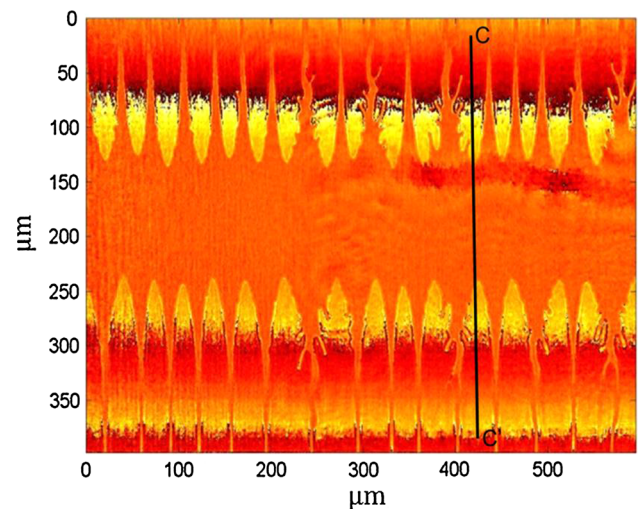

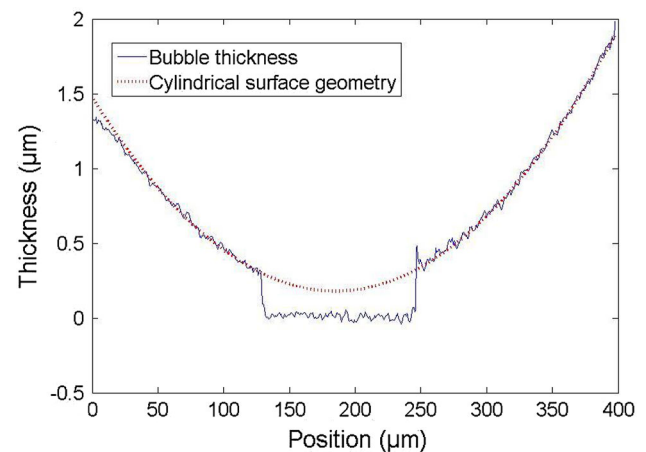Fig. 10 Addition of forward and reverse phase maps

Fig. 11 Bubble thickness measurement with reference to the cylindrical surface

the case of a sliding contact at 2 mm/s. Two conclusions can be drawn from these images. First, at lower velocities, the cavitation is more irregular with "fern-like fronds" or "fingers" that grow from the leading edge of the bubble and protrude towards the minimum clearance. The fern-like cavitation is less prevalent at high velocities (above 2 mm/s). Second, it can be seen that as the speed decreases, the cavitation moves towards the line of minimum clearance. This characteristic feature can be compared with the predictions of the various cavitation models as follows.

It can also be observed that as the sliding speed increases, the frequency of bubbles reduces while the gap between the bubbles increases. At 0.5 mm/s, the bubbles merge as the contact diverges with all the oil exiting the contact above or below the cavitated region (as predicted by Coyne and Elrod). As the speed of lubricant entrainment increases, the width of the lubricant steamers also increases
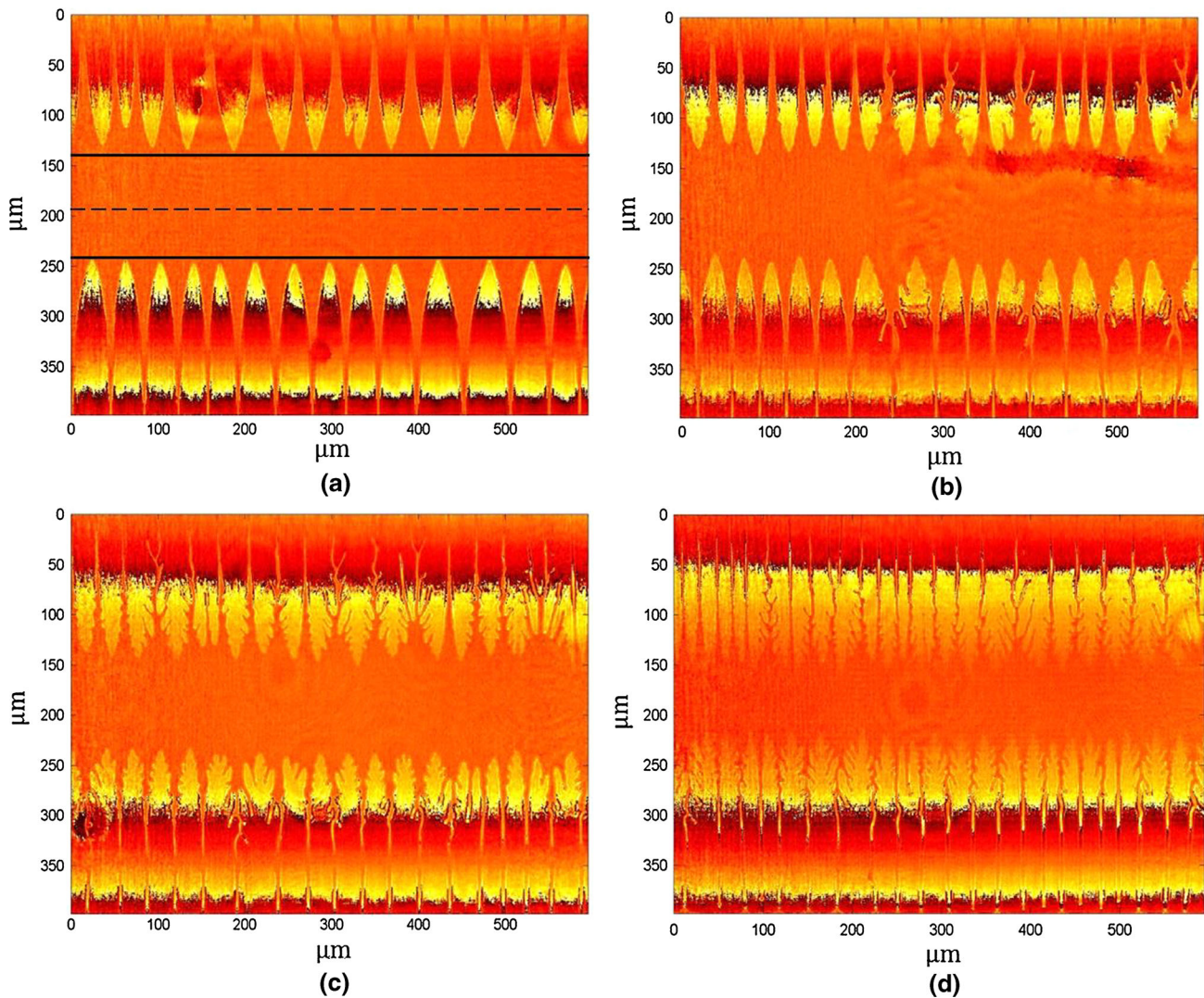
Fig. 12 Addition of forward and reverse phase maps at: **a** 2.0 mm/s; **b** 1.5 mm/s; **c** 1.0 mm/s; **d** 0.5 mm/s

indicating an increased mass flow exiting the contact through this mechanism. With the addition of minimum film thickness measurements, in future it will be possible to determine the exact proportions of oil exiting the contact through different mechanisms.

4.3 Comparison with Cavitation Models

The following section compares the position of film rupture (indicated by the leading edge of the cavitation bubbles) with that predicted by the various cavitation models. For a contact with constant load and speed, where there is minimal side leakage and the lubricating film is considered as an incompressible Newtonian fluid with a laminar entrainment, Reynolds equation can be used to determine the generated hydrodynamic pressures:

$$\frac{\partial}{\partial x}\left(h^3 \frac{\partial p}{\partial x}\right) = 6\eta U \frac{\partial h}{\partial x} \tag{5}$$

Despite the high-viscosity oil used in the current study, the slow sliding speed means that it is reasonable to assume that viscous heating in the contact can be assumed to be negligible. It should be noted, however, that at higher sliding speeds, thermal effects as a result of viscous heating could have a significant effect on the cavitation phenomena.

Following a similar procedure explained by Acoumanis [32] and others, the Reynolds equation can be integrated and simplified. The inlet pressure $p = p_{in}$ at $x = -b/2$ where b is a 1 mm central section of the cylinder considered in the analysis. For a sliding contact with profile $h(x)$ and a relative velocity U that is fully flooded with a lubricant of viscosity η, the resulting relationship can be obtained to determine where $x = x_{cav}$:

$$(6-k)U\eta h(x) + \frac{P_{\text{cav}} - P_{\text{in}} - 6\eta U \int_{x_{\text{in}}}^{x} \frac{1}{h^2(x)}\,\mathrm{d}x}{\int_{x_{\text{in}}}^{x} \frac{1}{h^3(x)}\,\mathrm{d}x} = 0 \qquad (6)$$

where k is a constant selected as follows in accordance with the cavitation models:

$$\text{Swift}[9]-\text{Steiber}[10] \quad k = 0 \qquad (7)$$

$$\text{Separation boundary}[18] \quad k = 2 \qquad (8)$$

$$\text{Elrod and Coyne}[19, 20] \quad k = 6\left(1 - 2\frac{h_{\infty}}{h}\right) \qquad (9)$$

It is noted that for the Elrod and Coyne model, a contact angle of $\pi/2$ is assumed and the ratio h/h_{∞} was calculated as a function of the capillary number $N = \left(\frac{3\eta U}{\gamma}\right)^{1/3}$ using curve fits produced by Priest et al. [33] for the experimental work of Taylor [34].

The JFO theory is slightly more complex as it requires consideration of a reformation boundary and allows for mass conservation in a dynamically loaded bearing. Elrod and Adams [15] and Elrod [16] developed a universal form of the Reynolds equation to implement the full JFO theory (Jacobson and Floberg [12] and Olsson [13]). In this case, an analytical method described by Sawicki and Yu [35] finds a solution to Elrod's (JFO) cavitation model.

As in the experimental measurements, a constant load, $W = 2.65\ N$, is applied to the contact and the hydrodynamic lift, F, must equal this force.

$$F = \int p\,\mathrm{d}A \qquad (10)$$

The minimum film thickness, h_m, is not known, and in order to calculate the rupture point for each of the models, it is necessary to adjust this parameter in an iterative manner, to change the pressure distribution and ultimately balance the load. In order to perform this function, a dimensionless merit function, ε, is defined such that,

$$\varepsilon = \left|\frac{W - F}{F}\right| \qquad (11)$$

In this study, a load convergence criteria is set such that if $\varepsilon \leq 10^{-4}$, the process is deemed to have converged to a solution and the process is complete. However, if the convergence criterion is not satisfied, then h_m is adjusted such that

$$h_m^{n+1} = (1 + \xi\chi)h_m^n \qquad (12)$$

where n is a counter of each iteration, the damping coefficient is $\xi = 5 \times 10^{-3}$ and $\chi = \frac{W-F}{\max\{W,F\}}$. In this way, a new hydrodynamic load-carrying capacity at the updated minimum film thickness is calculated and the process is repeated until convergence.

The position of the film rupture, as described in the previous section, is plotted and compared with the predictions of the various models in Fig. 13. It is noted that with the exception of the JFO theory, it has been assumed in the current paper that the cavity is at ambient pressure. If this condition is applied to the JFO theory, then the result exactly matches the Swift–Stieber result. The JFO position is reported for a lowered cavity pressure for $P_{\text{cav}} = 0.02$ MPa as used by Chong et al. [36] as the model allows for lubricant film reformation. The other boundary conditions do not consider lubricant film reformation and therefore the physical interpretation of this is that the cavity is open and exposed to the ambient pressure.

It can be seen that the various theories all indicate that the bubble position increases with higher lubricant entrainment to the contact, as is found in practice. However, predictions of the bubble position using the theories that imply flow over a single cavity, specifically those of Birkhoff and Hays and Coyne and Elrod, depart significantly from the experimental results. The experimental results appear to match more closely with the theories that assume that the lubricant flows around multiple cavities, those of the Swift–Stieber result and JFO theories.

It is instructive therefore to consider the minimum clearance h_m shown in Fig. 14. It can be seen that there is significant discrepancy in the load-carrying capacity between the theories. The difference in cavity pressures used in the Swift–Stieber and JFO predictions moves the film rupture point a little; however, this is accompanied by a large change in the minimum clearance. This is as a result of a decrease in the load-carrying capacity due to the negative gauge pressures sustained in the divergent section of the contact.

The range of film thickness presented by the models in real rough contacts would result in significant differences in the boundary and viscous friction. Therefore, the selection of appropriate exit boundary conditions which are applicable to the contact in question is paramount for the prediction of key bearing characteristics such as load-
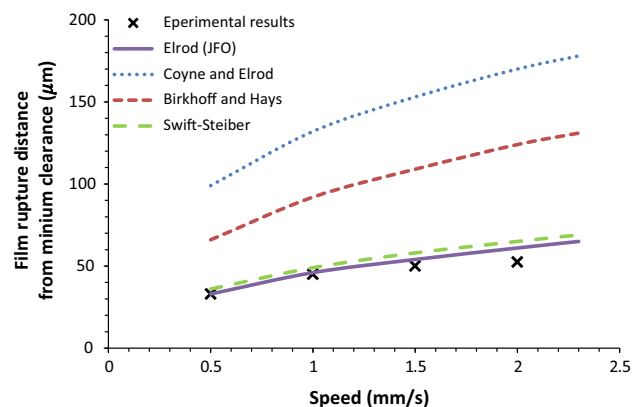

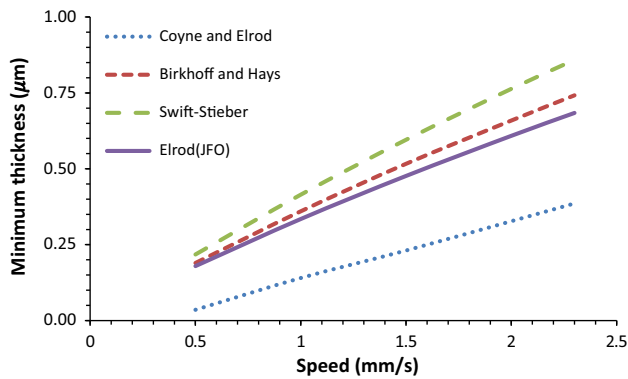Fig. 13 Bubble formation position versus speed

Fig. 14 Minimum thickness versus speed

carrying capacity and friction. It is concluded that the position of film rupture at a known load condition is not sufficient to validate the theories completely.

5 Conclusions

The paper has presented, for the first time, precise measurement of cavitation bubbles using digital holographic microscopy. The measurements are carried out for a high-viscosity lubricant intervening between cylindrical and sliding plane glass components. The benefit of using digital holography instead of incoherent imaging methods is that digital holography records both the phase and amplitude of the transmitted wavefront. Using this information, it is possible to make high-resolution measurements of bubble thickness and position.

The data from the phase images show that lubricant flows between the cavitation bubbles as predicted by the "multiple-cavity" assumption models, expounded by Swift–Stieber result and the JFO assumptions. Analysis of the high-resolution thickness measurements shows that the bubble thickness profile follows the curvature of the cylindrical bearing surface. Closer inspection, however, suggests that a thin film of lubricant flows over (or under) the cavitation bubbles as suggested by the "single-cavity" assumption of Birkhoff and Hays and Coyne and Elrod. Considering the pressure equilibrium between the inside and outside the bubble, it is clear that the bubble must be in contact with at least one of bearing surfaces. In this case, the results suggest that the bubbles are in contact with the cylindrical bearing surface. In conclusion, there is evidence for aspects of both the single- and multiple-cavity theories.

The experimental configuration allows for the control of speed and direction of the lubricated bearing surfaces. Using an argument based on symmetry, it was possible to measure the bubble formation position with respect to the minimum clearance position. A comparison with a

selection of widely used cavitation models has been made, the results showing that the multiple-cavity theory (JFO) is the best prediction for the low load, low speed conditions as in the current study. It is noted, however, that the results are taken at steady-state conditions, the constant film thicknesses produced by these conditions vary considerably amongst the models presented. It is, therefore, concluded that the position of bubble formation should not be the only discriminant and cannot be solely used to validate the predictive models reliably. For this reason, further work is planned to make simultaneous measurement of bubble and lubricant film thickness.

References

1. Dowson, D.: History of Tribology. Longman, London (1979)
2. Braun, M.J., Hannon, W.M.: Cavitation formation and modelling for fluid film bearings: a review. Proc. Inst. Mech. Eng. J J. Eng. Tribol. **224**(9), 839–863 (2010)
3. Wilson, R.W., Shone, E.B.: The diagnosis of plain bearing failures. Tribol. Ser. **8**, 80–131 (1983)
4. Dellis, P., Arcoumanis, C.: Cavitation development in the lubricant film of a reciprocating piston-ring assembly. Proc. Inst. Mech. Eng. J J. Eng. Tribol. **218**(3), 157–171 (2004)
5. Reynolds, O.: On the theory of lubrication and its application to Beauchamp Tower's experiments, including an experimental determination of the viscosity of olive oil. Philos. Trans. R. Soc. Lond. Ser. A **177**, 157–233 (1886)
6. Dowson, D., Taylor, C.M.: Cavitation in bearings. Annu. Rev. Fluid Mech. **11**(1), 35–65 (1979)
7. Majumdar, B.C., Brewe, D.E., Khonsari, M.M.: Stability of a rigid rotor supported on flexible oil journal bearings. J. Tribol. **110**(1), 181–187 (1988)
8. Gümbel, L.K.R.: Vergleich der Ergebrusse der rectinerischen Behandling des Lagerschmierangsproblem mitneueren Versuchsergebrussen. Monatsbl. Berliner Bez Ver. Dtsch. Ing. Sept. 125–128 (1921)
9. Swift, W.: The stability of lubricating film in journal bearing. J. Inst. Civ. Eng. **233**(1), 267–288 (1933)
10. Stieber, W.: Das Schwimmlager. Ver. Dtsch. Ing, Berlin (1933)
11. Floberg, L.: On journal bearing lubrication considering the tensile strength of the liquid lubricant. In: Vedmar, L. (ed.) Transactions of the Machine Elements Division, pp. 1–26. Lund Technical University, Lund, Sweden (1973)
12. Jakobson, B., Floberg, L.: The finite journal bearing considering vaporization. In: Transactions Chalmers University of Technology, Guthenberg, Sweden, vol. 190, pp. 1–119 (1957)
13. Olsson, K.O.: Cavitation in Dynamically Loaded Bearings, p. 308. Transactions of Chalmers University Technology, Goteborg (1965)
14. Floberg, L.: Cavitation boundary conditions with regard to the number of streamers and tensile strength of the liquid. In: Dowson, D., Godet, M., Taylor, C.M. (eds.) Cavitation and

Related Phenomena in Lubrication, Proceedings of the 1st Leeds–Lyon Symposium on Tribology, pp. 31–36. University of Leeds, Leeds (1974)

15. Elrod, H.G., Adams, M.: A computer program for cavitation and starvation problems. In: Dowson, D., Godet, M., Taylor, C.M. (eds.) Cavitation and Related Phenomena in Lubrication, Proceedings of the 1st Leeds–Lyon Symposium on Tribology, pp. 37–41. University of Leeds, Leeds (1974)

16. Elrod, H.G.: A cavitation algorithm. J. Tribol. **103**(3), 350–354 (1981)

17. Vijayaraghavan, D., Keith Jr, T.G.: Development and evaluation of a cavitation algorithm. Tribol. Trans. **32**(2), 225–233 (1989)

18. Birkhoff, G., Hays, D.F.: Free boundaries in partial lubrication. J. Math. Phys. **42**(2), 126 (1963)

19. Coyne, J.C., Elrod, H.G.: Conditions for the rupture of a lubricating film. Part I: theoretical model. J. Tribol. **92**(3), 451–456 (1970)

20. Coyne, J., Elrod, H.G.: Condition for the rupture of a lubricating film-part II: new boundary condition for Reynolds equation. J. Lubr. Technol. **93**, 156 (1971)

21. Groper, M., Etsion, I.: The effect of shear flow and dissolved gas diffusion on the cavitation in a submerged journal bearing. J. Tribol. **123**(3), 494–500 (2001)

22. Dowson, D., Smith, E.H., Taylor, C.M.: An experimental study of hydrodynamic film rupture in a steadily-loaded, non-conformal contact. J. Mech. Eng. Sci. **22**(2), 71–78 (1980)

23. Etsion, I., Ludwig, L.P.: Observation of pressure variation in the cavitation region of submerged journal bearings. J. Tribol. **104**(2), 157–163 (1982)

24. Dowson, D.: Cavitation in lubricating films supporting small loads. In: Proceedings of Institutional of Mechanical Engineering Conference Lubrication and Wear, pp. 93–99 (1957)

25. Braun, M.J., Hendricks, R.C.: An experimental investigation of the vaporous/gaseous cavity characteristics of an eccentric journal bearing. ASLE Trans. **27**(1), 1–14 (1984)

26. Heshmat, H.: The mechanism of cavitation in hydrodynamic lubrication. Tribol. Trans. **34**(2), 177–186 (1991)

27. Arcoumanis, C., Duszynski, M., Flora, H., Ostovar, P.: Development of a piston-ring lubrication test-rig and investigation of boundary conditions for modelling lubricant film properties (No. 952468). SAE Technical Paper (1995)

28. Vladescu, S.C., Olver, A.V., Pegg, I.G., Reddyhoff, T.: The effects of surface texture in reciprocating contacts-an experimental study. Tribol. Int. **82**, 28–42 (2015)

29. Wormald, S.A., Coupland, J.M.: Particles image identification and correlation analysis in microscopic holographic particle image velocimetry. Appl. Opt. **48**(33), 6400–6407 (2009)

30. Lobera, J., Coupland, J.M.: Contrast enhancing techniques in digital holographic microscopy. Meas. Sci. Technol. **19**(2), 025501 (2008)

31. Laplace, P.S.: Mécanique Céleste: 8th book. Theory of the satellites of Jupiter, Saturn, and Uranus. 9th book. Theory of comets. 10th book. On several subjects relative to the system of the world. Supplement to the tenth book: on capillary attraction. Supplement to the theory of capillary attraction, Vol. 4. Hillard, Gray, Little, and Wilkins (1839)

32. Arcoumanis, C., Duszynski, M., Flora, H., Ostovar, P.: Development of a piston-ring lubrication test-rig and investigation of boundary conditions for modelling lubricant film properties (No. 952468). SAE Technical Paper (1995)

33. Priest, M., Dowson, D., Taylor, C.M.: Theoretical modelling of cavitation in piston ring lubrication. Proc. Inst. Mech. Eng. C J. Mech. Eng. Sci. **214**(3), 435–447 (2000)

34. Taylor, G.I.: Cavitation of a viscous fluid in narrow passages. J. Fluid Mech. **16**(04), 595–619 (1963)

35. Sawicki, J.T., Yu, B.: Analytical solution of piston ring lubrication using mass conserving cavitation algorithm. Tribol. Trans. **43**(4), 587–594 (2000)

36. Chong, W.W.F., Teodorescu, M., Vaughan, N.D.: Cavitation induced starvation for piston-ring/liner tribological conjunction. Tribol. Int. **44**(4), 483–497 (2011)